Echo tracer dispersion in model fractures with a rectangular geometry[1]

I. Ippolito[a], G. Daccord[b], E.J. Hinch[c], J.P. Hulin[a]

[a]*Laboratoire de Physique et Mécanique des Milieux Hétérogènes (URA-CNRS No. 857), ESPCI, 10 rue Vauquelin, F-75231 Paris Cedex 05, France*

[b]*Schlumberger Dowell, ZI de Molina la Chazotte, BP90, F-42003 Saint-Étienne Cedex 1, France*

[c]*Department of Applied Mathematics and Theoretical Physics, University of Cambridge, Silver Street, Cambridge CB3 9EW, UK*

Abstract

We report an experimental study of tracer dispersion in model rectangular fractures with rough or smooth walls and with different mean apertures. We use an echo dispersion technique in which tracer is first injected into the fracture and then pumped back through a detector.

In a parallel flow regime, echo dispersion combines a geometrical mechanism due to the fracture roughness and a Taylor mechanism related to the parabolic velocity profile between walls. The latter effect is dominant at high velocities and the dispersivity variations with velocity allow one to determine the effective aperture of the fracture. The low-velocity dispersivity limit that should be related to the geometrical characteristics of the roughness was found to be independent of the mean fracture thickness for the two models that were studied.

We show experimentally and numerically that velocity variations in the direction perpendicular to the flow lines result in additional dispersion resulting from molecular diffusion of the tracer particles across the flow lines.

1. Introduction

1.1. Objectives of the study

The study of fluid flow and mass transfer in fractured rocks and materials is a challenging fundamental problem because of the strong heterogeneities generally present in these media. Fractured structures display often a broad range of

characteristic length scales and their transport properties depend very much on the connectivity and the spatial distribution of the flow paths. Such heterogeneities strongly influence the velocity field and the transport properties. Heterogeneities may be present both at the scale of individual fractures (Silliman, 1989) and at the scale of the fracture network (Charlaix et al., 1987). In the latter case, the degree of connectivity often plays an important part and percolation-like effects (Charlaix et al., 1984) may be observed. In many cases fluid transport takes place through preferred paths, and channel flow models (Moreno et al., 1988) describe well transport mechanisms through a single fracture or a network of fractures.

In the present study, we concentrate on the experimental characterization of local geometrical parameters of a single fracture such as its mean aperture and its roughness by using tracer dispersion. For that purpose, we have performed echo tracer dispersion measurements on various individual model fractures with controlled characteristics: in this technique (Hulin and Plona, 1989), tracer is first injected into the fracture during a preselected time and then pumped back through a detector. Compared with classical transmission dispersion, this method reduces strongly the influence of the length and velocity differences between the various flow paths. This allows one to obtain information on the local structure complementing that resulting from classical transmission dispersion measurements.

Let us emphasize that the study of fractured media has many practical applications in the domains of hydrogeology and geothermics (Evans et al., 1992), as well in those of petroleum, chemical and nuclear engineering or waste management: the influence of the flow field heterogeneities and of the local structure of the fractures will be very significant in these problems.

In the following, we call fractures the space between two parallel smooth or rough solid surfaces. We shall always assume that this space is completely saturated with fluid. We use model fractures with well-controlled geometries in order to analyse the relation between the dispersion characteristics, the mean aperture a of the fractures and their roughness.

We first present our experimental tool. Tracer dispersion has been selected because of its high sensitivity to flow heterogeneities and to spatial velocity variations.

1.1. Tracer dispersion and its different mechanisms

First recall some basic results of tracer dispersion in media of various geometries. In homogeneous systems where the fluid has a uniform velocity U in the x-direction, the variation of the tracer concentration C should satisfy the classical advection–diffusion equation (Bear, 1972; Dullien, 1979):

$$\frac{\delta C}{\delta t} + U\frac{\delta C}{\delta x} = D_{\parallel}\frac{\delta^2 C}{\delta x^2} + D_{\perp}\left[\frac{\delta^2 C}{\delta y^2} + \frac{\delta^2 C}{\delta z^2}\right] \tag{1}$$

where $D_{\parallel}$ and $D_{\perp}$ are the longitudinal and transverse dispersion coefficients, respectively; x corresponds to the direction parallel to the velocity U, while y and z are perpendicular to U. Generally, both the values of $D_{\parallel}$ and $D_{\perp}$ depend on U. In the following, we shall assume that concentration is uniform in the direction

perpendicular to the flow and neglect the transverse dispersion term except when otherwise stated. Eq. 1 applies only if individual events indu ing a spreading of the tracer have a short duration compared to the global transit time in the sample (this allows the central limit theorem to be applied).

In three-dimensional (3-D) porous media such as homogeneous packings of grains of uniform size, $D_{\parallel}$ is roughly proportional to the velocity U (Saffman, 1959; Pfann-kuch, 1963; Fried and Combarnous, 1971) for Péclet number values Pe > 10 (Pe = Ud/D_m, where d is the typical grain size and D_m is the molecular diffusion coefficient). Then one has:

$$l_D = D_{\parallel}/U \tag{2}$$

where the *dispersivity*, l_D, is nearly constant with respect to the velocity U and is of the order of $d/2$ for homogeneous packings. In this case, the dominant dispersion mechanism (called geometrical dispersion) is the variation of the velocity of the tracer particles as they move from one pore channel to another. Their trajectory can be pictured as a random walk through the sample superimposed on a mean drift motion. l_D is then the length of an individual step of the random walk and the spatial disorder of the pore space structure is the key factor controlling dispersion.

On the other hand, in ordered flow geometries such as capillary tubes, dispersivity is due to the fluid velocity differences associated with the Poiseuille parabolic profile in the flow section: the tracer motion is obviously much slower near the walls than at the center of the capillary tube. This spreading is limited by transverse molecular diffusion across the tube section which continuously exchanges tracer between slow and fast zones. In this mechanism, called Taylor dispersion, the dispersion coefficient $D_{\parallel}$ varies as the square of the mean velocity U at high Péclet numbers. For a capillary tube of diameter d, one has (Taylor, 1953; Aris, 1956):

$$D_{\parallel} = d^2 U^2 / 192 D_m + D_m \tag{3}$$

Note that the characteristic molecular diffusion time *across* the capillary tube section is $\tau_m = d^2/D_m$. The dispersivity l_D may then be expressed:

$$l_D = D_{\parallel}/U = U\tau_m/192 + D_m/U \tag{4}$$

The second term in Eq. 4 corresponds to pure longitudinal molecular diffusion and is only significant at low Péclet numbers (Pe = $Ud/D_m \leqslant 10$). At high velocities, it becomes negligible and $l_D \cong (U\tau_m/192)$. Thus, in order to describe Taylor dispersion by a random walk model like geometrical dispersion, $U\tau_m$ needs to be considered as the typical path distance travelled before a tracer particle diffuses by a significant fraction of the diameter d from its initial location in the tube section. Thus, after the time τ_m has elapsed, the velocity of the tracer particle parallel to the tube axis is not correlated any more to its initial value.

For a fracture with smooth parallel walls, Taylor dispersion and longitudinal molecular diffusion are the only effective dispersion mechanisms in the same way as in capillary tubes. The dispersivity is given by:

$$l_D = D_{\parallel}/U = U\tau_m/210 + D_m/U = Ua^2/210D_m + D_m/U \tag{5}$$

where a is the distance between the walls (fracture aperture); $\tau_m = a^2/D_m$; and the coefficient 210 replaces 192 in Eq. 4 because of the planar geometry (Aris, 1956). If one or both walls are rough, there will be some disorder in the flow field, particularly if the height of the asperities is comparable to the fracture aperture. A dispersion mechanism analogous to geometrical dispersion due to the random splitting of the flow tubes is then present. Roughness mostly introduces a two-dimensional (2-D) disorder in planes parallel to the fracture surface but does not move tracer away from or towards the solid surfaces. Thus, we may expect that the effect of wall roughness will be not to suppress Taylor dispersion but rather to be superimposed on it.

In the following we shall first present our experimental set-up and the data processing procedure. We shall then analyse the dependence of dispersion on flow velocity, fracture aperture and wall roughness. We shall particularly seek the relative influence of the geometrical and Taylor dispersion mechanisms. Finally, we shall discuss how velocity gradients in the plane of the fracture (due to thickness variations and velocity gradients near the injection point) may influence the dispersion.

2. Experimental procedure

2.1. Model fracture

The smooth model fracture we used corresponds to the gap between two rectangular parallel flat glass plates (1 m × 0.15 m). Rubber spacers 10 mm wide and of thickness 0.5 or 1 mm are placed at the rim of the model to give a constant aperture (Fig. 1). A Silicone[R] seal is then made all around the perimeter of the model to produce a leak-free assembly.
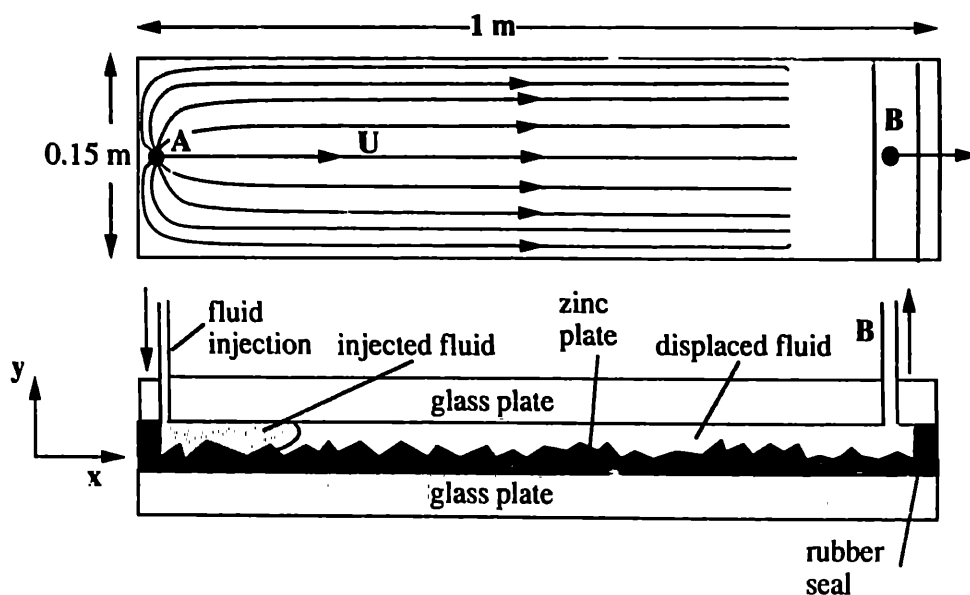

Fig. 1. Schematic view of the model rectangular fracture:
a. View from above with mean flow lines.
b. Side view with enlarged length scale in the direction perpendicular to the plates.
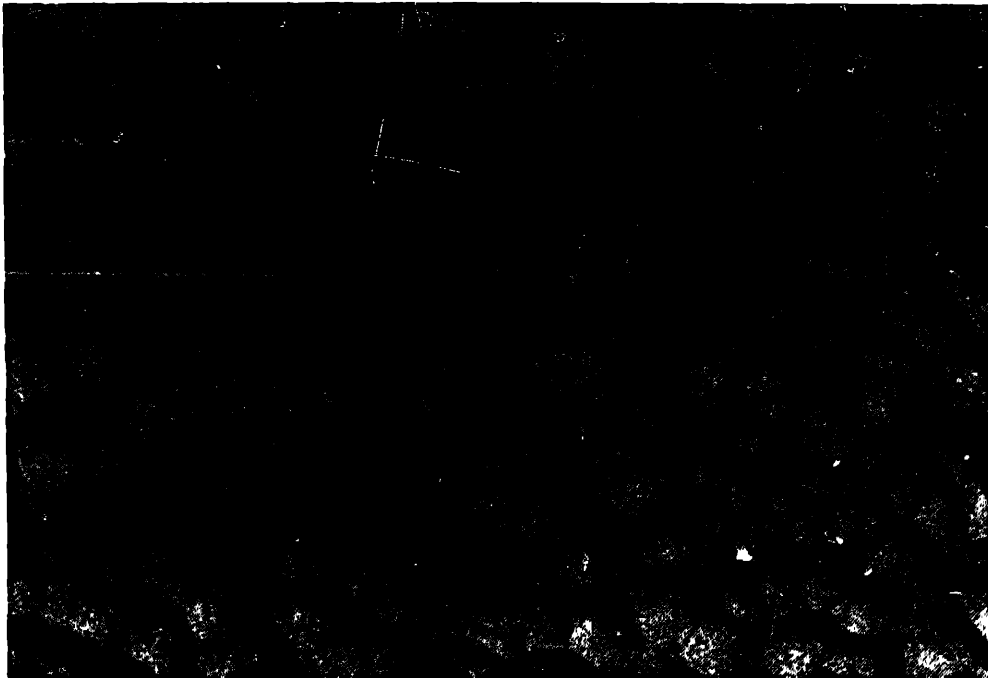
Fig. 2. Micrograph view of the rough etched zinc plate (the field of view is 25 × 17 mm).

The rough fractures use a modified assembly in which a rough zinc plate is glued onto one of the glass planes (Fig. 1). The asperities have a typical height of 1 mm; their average spacing is also of the order of 1 mm (Fig. 2). The predefined roughness pattern is generated by computer and then printed onto a photosensitive protective varnish covering the zinc plate; then the plate is etched selectively by an acid solution.

Fluid is injected (or pumped back) locally at a point A placed on the axis of the model at 10 mm of one end: it flows out (or enters) at the other end where a 1-mm-deep rectangular channel has been milled in order to distribute evenly the flow (a small tube is connected to this channel at point B). This configuration produces a nearly parallel flow field in the outlet region. From the hydrodynamic point of view, the model has a flow field initially radial (slightly influenced by the injection details) which becomes parallel after a path length of the order of the width of the model: thus the modulus of the local velocity V (averaged over the spacing between plates) first decreases with the radial distance from the injection point and then becomes uniform and constant.

2.2. Tracer dispersion measurements

In the echo technique which we used, the tracer solution is first injected into the fracture and then pumped back through a detector (Hulin and Plona, 1989) located close to the injection point A. Such measurements strongly reduce the effect of the differences between the macroscopic flow paths. During an echo experiment, tracer particles located on the fastest flow paths move farthest during the injection part; however, they return to the detector close to A at the same mean time as particles on the slowest paths. In this case, the width of the transit time distribution is due to

smaller-scale effects and is controlled by the local structure of the fracture. On the other hand, transmission measurements between points A and B would be controlled by the difference of transit times between the direct fast path and those flowing near the edges of the model. Such contrasts between the macroscopic transit times along various flow paths are also observed in stratified media (Leroy et al., 1992) or in dipole flow geometries (Kurowski et al., 1994).

Practically, we use a salt solution ($NaNO_3$) as a tracer; we detect the variations $C(t)$ of the concentration at the inlet, using a conductivity measurement and a low volume detector connected to the injection point A. A steady flow of a salt solution of concentration C_1 is initially established by a double syringe pump. Then an abrupt change of the concentration of tracer is induced by keeping the flow rate constant but connecting the inlet to the second syringe filled with a different solution C_2. After a predetermined time, T_{inv}, following the concentration variation, we reverse the flow and $C(t)$ is monitored while the mixture of the two solutions moves out of the system. In this way, we obtain after a time of the order of $2T_{inv}$ an echo signal at the detector. A typical experimental curve is shown on Fig. 3a. The mean penetration depth of the tracer into the fracture can be adjusted by varying T_{inv}. Note that curves obtained with this step variation of concentration are the integrals of the variations of $C(t)$ corresponding to a pulse of short injection. This follows from the fact that the tracer transport equations are linear in the concentration, that we use a linear detection technique and that no noticeable adsorption occurs.

2.3. Analysis of the tracer dispersion curves

We have made measurements for a large range of penetration lengths (or injection times T_{inv}) and for 9 different flow-rates Q ranging between 0.53 and 213 $mm^3\,s^{-1}$. All these studies were performed in a smooth model with a mean aperture $a = 1$ mm and rough models using the same rough zinc plate with $a = 1$ and 0.5 mm.

The experimental curves are fitted with Gaussian solutions of the advection–diffusion equation (1) (Bear, 1972). We have computed the corresponding first and second moments of the tracer transit time distribution $\overline{T}$ and $\sigma_t^2 = (\overline{T^2}) - (\overline{T})^2$. The variation of the first moment is used to verify that all the tracer injected into the model is actually recovered: in this case, the mean transit time $\overline{T}$ must be equal to $2T_{inv} + K$ (K is a small additive constant corresponding to the dead volume of the injection circuit; Hulin and Plona, 1989). We have verified this condition with a precision of $\sim \pm2\%$ by plotting the variations of $\overline{T}$ with T_{inv} and performing a linear regression.

The second moment σ_t^2 of the tracer time distribution characterizes the tracer dispersion. For a uniform and constant flow velocity U, σ_t^2 is related to the longitudinal dispersion coefficient $D_\parallel$ and to the dispersivity l_D by (Koplik, 1988):

$$D_\parallel = \frac{U^2}{2}\frac{\sigma_t^2}{\overline{T}} \qquad \text{or} \qquad l_D = \frac{U}{2}\frac{\sigma_t^2}{\overline{T}} \tag{6}$$

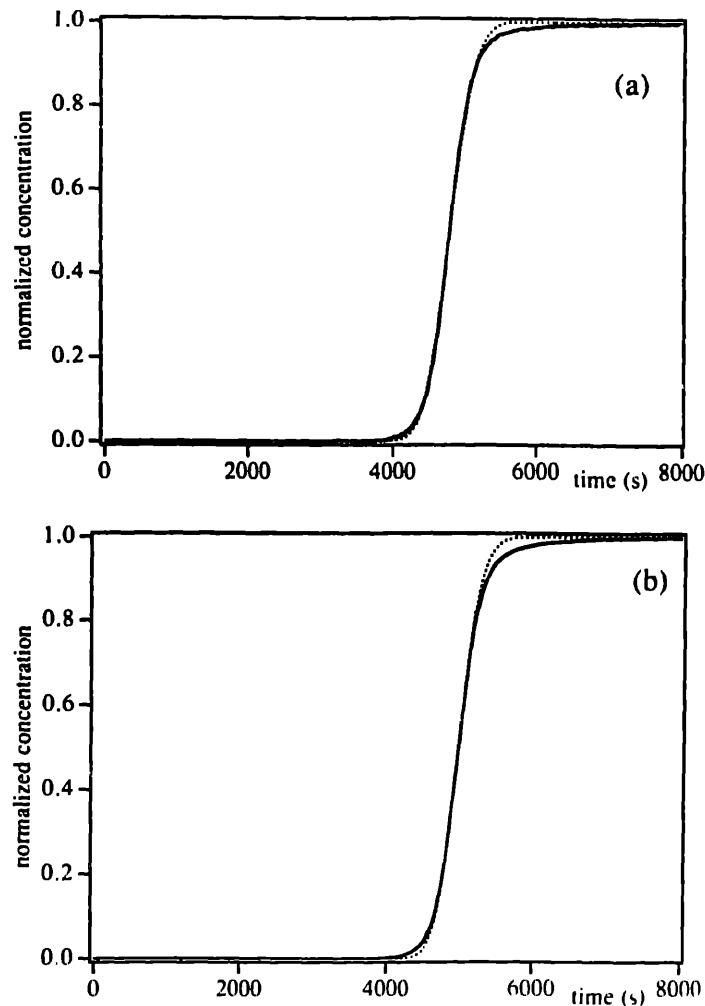For the flow geometries shown in Figs. 1 and 7, the velocity varies with distance along

Fig. 3. Time variation of the normalized concentration $C(t)$ in an echo experiment performed after a step change at the inlet for a Péclet number Pe = 34:

a. Experimental variation observed for an inversion time Tinv = 2400 s.

b. Theoretical variation obtained from a numerical simulation with T_{inv} = 2500 s.

In both cases, the *dotted lines* correspond to a best fit of the experimental data with a "Gaussian" solution of the advection-diffusion equation.

the flow paths and also across the streamlines. The second moment σ_t^2 then corresponds to an integral:

$$\sigma_t^2 = \left\langle \int \frac{d\sigma_t^2}{dt} dt \right\rangle = \left\langle \int_0^t \frac{2l_D[V(t)]}{V(t)} dt \right\rangle \tag{7}$$

where the ensemble averages $\langle\ \rangle$ are taken over all the streamlines. Let us remark that we have chosen to take the integral of the transit time deviation σ_t^2 and not that of the spread σ_x^2 in distance. Deviations of the transit time acquired during one part of the path are indeed conserved as the velocity varies along the path of a fluid particle: on the other hand, deviations in distance parallel to the flow are stretched and compressed in a ratio proportional to the flow velocity. Rigorously, the various contributions to the value of σ_t^2 only add up if the various flow sections are independent and

the particles lose their memory as they pass from a flow section to the next (Leven-spiel, 1972). Practically, this implies that, for Eq. 7 to apply at all times, the velocity variations during the transverse diffusion time τ_m must be small.

This condition will be particularly easy to fulfil at sufficiently long times when the concentration front reaches the parallel flow zone: in this case, the fluid velocity has a constant value U and $l_D(U)$ is constant. In this situation, the local dispersivity should take the same value $l_D(U)$ for all particles. For two large mean transit times, $\overline{T_1}$ and $\overline{T_2}$, one should have therefore:

$$\sigma_t^2(\overline{T_2}) - \sigma_t^2(\overline{T_1}) = \frac{2l_D(U)}{U}(\overline{T_2} - \overline{T_1}) \tag{8}$$

σ_t^2 should then vary linearly with the transit time at long times, allowing one to determine an effective value of the dispersivity from the slope of the curve. Even if the velocity variations are large at early times so that Eq. 7 does not remain valid close to the injection point: this will introduce only an additive term in σ_t^2 which will subtract out in Eq. 8 which remains therefore valid.

3. Dispersion measurements

3.1. Influence of roughness on echo dispersion

We see in Fig. 4 that the linear variation predicted by Eq. 8 is well verified for sufficiently large penetration depths (corresponding to a diffusive behaviour) both for the fracture with two smooth walls and the one with one smooth wall and one rough wall and with the same mean aperture $a = 1$ mm. On the other hand, at short penetrations lengths corresponding to the distances near the injection point (a few tens of mm), we observe a small deviation from the linear behaviour. We so remark
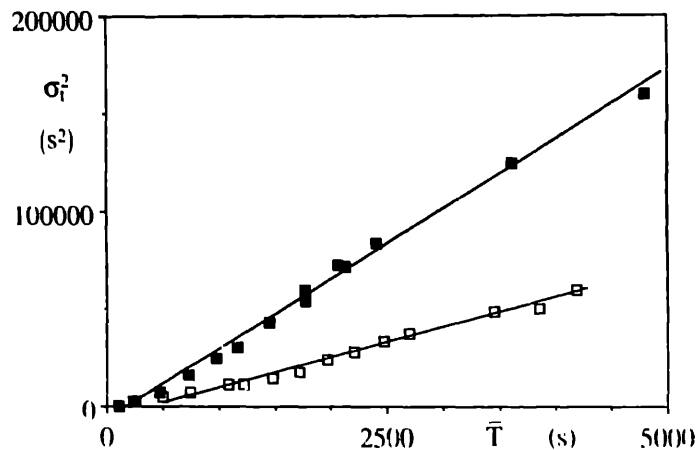

Fig. 4. Variation of the mean square deviation σ_t^2 of the residence time of the tracer particles in the fracture volume with the mean residence time, $\overline{T}$, at a Péclet number Pe = 50 ($\square$ = two smooth planes; $\blacksquare$ = one smooth plane and one rough zinc plate), mean aperture $a = 1$ mm. The *straight lines* correspond to a linear regression over all data points.
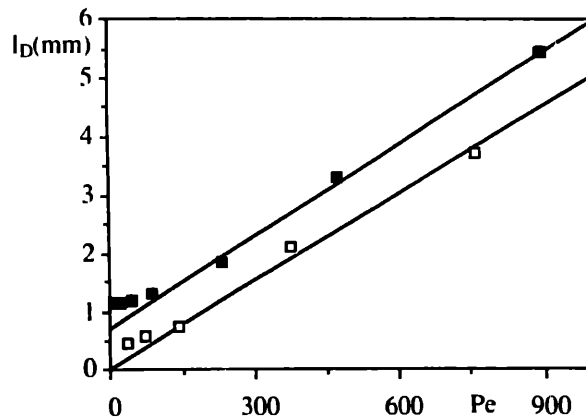
Fig. 5. Variation of the asymptotic dispersivity, l_D, as a function of the Péclet number Pe $= Ud/D_m$ for two model fractures with the same mean aperture $a = 1$ mm ($\square$ = fracture with two smooth parallel plane walls; $\blacksquare$ = fracture with one rough and one smooth wall). The *straight lines* correspond to linear regressions performed over data corresponding to Pe $\geqslant 100$.

in Fig. 4 that, at the Péclet number used in the experiment (Pe $\approx$ 50), the value of σ_t^2 for a given value of the transit time is twice as large for the rough fracture compared with the smooth one.

Using Eq. 8 we determine a dispersivity from the slopes of these curves. Fig. 5 shows the variation of this asymptotic dispersivity $l_D = D_{\parallel}/U$ with the Péclet number Pe between 10 and 900 for the two model fractures with the mean aperture $a = 1$ mm. The fractures correspond respectively to the smooth model ($\square$) and the rough one ($\blacksquare$) with the type of roughness shown in Fig. 2. The Péclet number was taken equal to Ua/D_m where D_m is the molecular diffusion coefficient ($D_m = 1.5 \cdot 10^{-9}$ m^2 s^{-1}) and the mean spacing between plates $a = 1$ mm is used as the characteristic length scale of the flow.

From Fig. 5, we observe for the smooth wall model that the dispersivity l_D is proportional to the Péclet number at high values of the Péclet number (Pe > 100) as expected for a pure Taylor dispersion mechanism.

A linear regression taken over Pe > 100 yields the following approximate dependence of dispersivity on velocity:

$$l_D = 0.85 + 5.2 \cdot 10^{-3} \text{Pe} \tag{9}$$

for the rough fracture and

$$l_D = 4.6 \cdot 10^{-3} \text{Pe} \tag{10}$$

for the smooth one.

From Eqs. 9 and 10, we observe that the mean slope of the variation of l_D with the Péclet number or the mean velocity flow U is about the same for the rough and the smooth fracture. The use of high-velocity points only allows one to eliminate the influence of transverse diffusion across the flow lines which will be discussed in Sections 4.1-3: this effect explains indeed the nonlinearities in the variation of l_D with Pe observed at low velocities.

In the smooth model fracture we can extrapolate $l_D \approx 0$ for Pe $= 0$. On the other

hand for the model with one rough wall, l_D still varies linearly with Pe but it extrapolates to a non-zero value $l_D \approx 0.85$ mm for Pe = 0. This non-zero value would correspond to a geometrical dispersion mechanism associated with the spatial disorder of the rough surface. Such a contribution is independent of the Péclet number as long as it is sufficiently large: the value of 0.85 mm is in reasonable agreement with the mean characteristic spacing of the asperities which is also of the order of 1 mm.

Let us compare now the relations (9) and (10) with the Taylor dispersivity l_D: rewriting Eq. 5 as a function of the effective aperture a_{eff} and the Péclet number Pe = Ua_{eff}/D_m and neglecting the longitudinal molecular diffusion term, we obtain: $l_D(Pe) \approx a_{eff}Pe/210$. This allows to estimate the value a_{eff} of the effective aperture a of the system: one finds $a_{eff} = 1.09$ and 0.97 mm, in the rough and smooth cases, respectively, close to the actual value 1 mm.

This indicates that the roughness does not influence the contribution of the Taylor mechanism which only depends on the mean aperture. Finally, let us remark that Fig. 5 displays at sufficiently low Péclet numbers a small upward deviation from the linear behaviour both for the smooth and the rough fracture model. We shall describe below a complete Monte Carlo simulation of the smooth model allowing us to interpret this deviation.

3.2. Influence of fracture aperture on echo dispersion for rough fractures

Let us analyse now how the dispersivity is modified when one varies the mean aperture for the model with one rough wall. We have performed for that purpose several echo experiments on a model using the same rough plate as above but with a different mean spacing a = 0.5 mm.

Fig. 6a and b displays the variations of l_D with the Péclet number in linear and logarithmic coordinates, respectively, for the two rough fractures of mean apertures a = 0.5 and 1 mm: both fractures have the same rectangular geometry and use the same rough zinc plate.

We observe that, at low Péclet numbers Pe < 95 (a = 0.5 mm) and Pe < 50 (a = 1 mm), l_D is about constant and equal to the same value l_D = 1 mm; this means that geometrical dispersion is dominant at low Pe numbers and that the limiting value $l_D \approx 1$ mm is related to the geometrical characteristics of the asperities of the plate. Let us note, however, that this limiting value is slightly higher than the extrapolation at Pe = 0 of the high-velocity variation (Fig. 6).

At high velocities, l_D varies linearly with Pe (or U) in both cases as expected for the Taylor dispersion mechanism. For a = 0.5 mm, one obtains:

$$l_D \approx 0.93 + 2.6 \cdot 10^{-3}Pe \tag{11}$$

The slope of the variation is, as expected, much smaller than that given by Eq. 9 for a = 1 mm. Let us note that longitudinal molecular diffusion is negligible in all experiments for Pe > 10. We obtain an effective aperture a_{eff} = 0.54 mm in good agreement with the actual value, as already mentioned for the other case a = 1 mm.
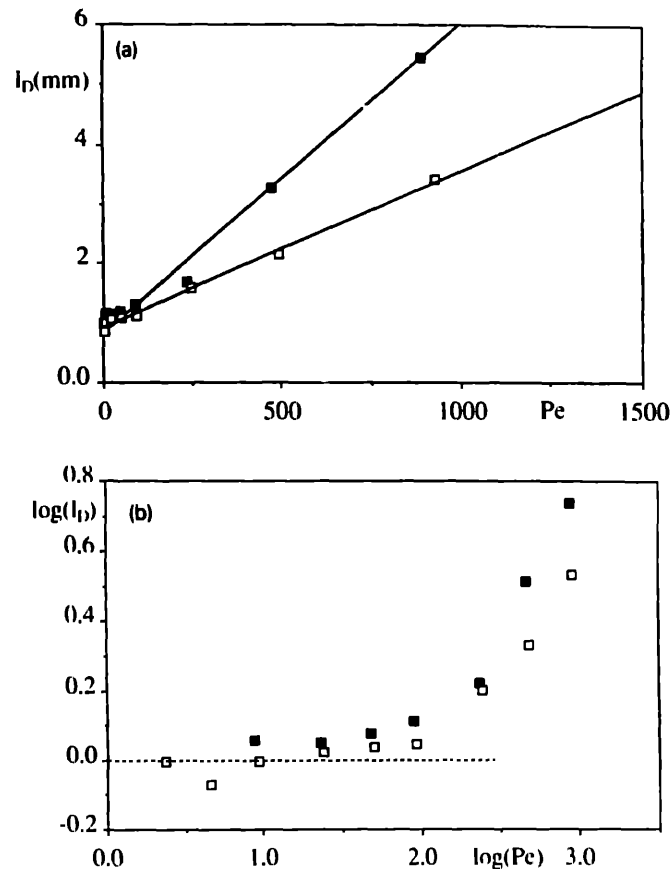
Fig. 6. Variation of the asymptotic dispersivity, l_D, in the parallel part of the flow field with the Péclet number Pe for $a = 0.5$ mm ($\square$) and $a = 1$ mm ($\blacksquare$). In both cases, one of the fracture walls is rough as shown in Fig. 2.

a. Linear coordinates.

b. Log-log axis coordinates (the value of l_D has been written in mm to compute the logarithm). The *dotted line* corresponds to $l_D = 1$ mm.

This confirms that Taylor dispersion is directly related to the spacing between plates.

3.3. Interpretation of echo dispersion measurements

The above results confirm that tracer dispersion in this type of fracture combines two mechanisms. The first is Taylor-like due to local velocity gradients normal to the wall. The second is geometrical due to the spatial variations of the velocity field in the directions parallel to the walls. The overall experimental dispersivity is the sum of these two contributions:

$$l_D = D/U \approx a^2 U/210 D_m + l_g + D_m/U \qquad (12)$$

where a is the mean aperture; U the mean velocity; D_m the molecular diffusion coefficient; and l_g is a characteristic length associated with the geometrical dispersion. The first term represents the Taylor mechanism and the last molecular

diffusion which is dominant only at very low velocities (we neglected it in the above sections).

Eq. 12 has been confirmed by comparing measurements on fractures of identical mean apertures but without roughness: the contribution of the Taylor mechanism is the same (linear increase of l_D with velocity) but the low-velocity limit of l_D (corresponding to geometrical dispersion) is very different. For the smooth fracture, l_D at $Pe = 0$ has a very low value, while for the rough model, l_D is of the order of the dimension of the asperities. We compared also the variations of l_D for rough models with different spacings: l_D increases faster with U when the spacing is higher while the low-velocity limit, determined by the roughness, is the same. Finally, the range of Péclet number values over which l_D is constant (geometrical dispersion) becomes broader as the spacing decreases. Let us remark that, in the geometrical dispersion regime, the dispersion characteristics are very similar to those of a 2-D system. At low flows, transverse molecular diffusion homogenizes the tracer concentration over the fracture thickness: then tracer dispersion is determined by spatial variations parallel to the plate.

A similar behaviour has been previously observed (Charlaix et al., 1988) on 2-D square lattices of channels of random widths, modelling a well-connected porous medium. In contrast with usual 3-D porous media, ones does not measure a constant dispersivity in this case but a linear increase of l_D with the mean velocity U as in Fig. 6. The physical origin of the effect is rather analogous. As in fractures, tracer particles that are close to the upper or lower solid walls of the 2-D model can only move away from them through molecular diffusion: these surfaces are continuous throughout the model.

We note that these measurements are much easier when the echo dispersion technique is used instead of the classical transmission method. Take the example already quoted in Section 2.2 of a tracer transmission experiment performed between localized injection and detection points. Then, the macroscopic differences between the various paths lengths are the dominant factor instead of geometrical and/or Taylor dispersion (Kurowski et al., 1994). In the echo measurement, the effect of differences in the path length is largely suppressed by the reversal of the flow field.

4. Numerical simulations

In Fig. 5, we have seen that the variation of dispersivity with the Péclet number deviated markedly at low velocities from the linear behaviour expected from Taylor dispersion mechanism. This feature is observed both for the smooth and the rough fracture so that the effect of geometrical dispersion cannot account for the phenomenon. We envision two explanations for this effect. Both are related to molecular diffusion across streamlines, a process ignored at the beginning of the paper.

One possible explanation is the influence of the velocity gradients in the region near the injection point and the edges of the rectangular model (Fig. 7). Until it reaches the parallel flow region, a particle located on a flow line close to the axis of the model will move a short distance at high velocity. On the other hand, a particle located on a flow
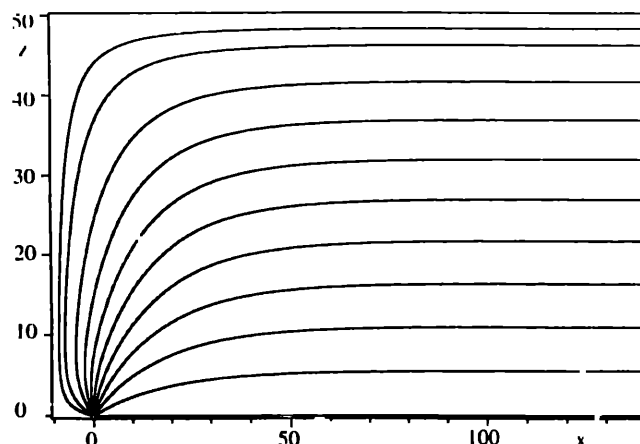
Fig. 7. Mean flow lines in the rectangular cell computed in the Hele–Shaw approximation (Eq. 13). Only one half of the whole cell is shown: the second one is symmetrical with respect to the axis $z = 0$. The space between all flow lines carries 5% of the total volume flow rate Q, while the two outermost ones carry 2.5% of Q each.

line going close to the edge has to travel for a longer distance at a lower velocity, particularly near the corner of the model. Molecular diffusion transverse to the flow lines may bring some tracer particles into very slow paths near the edges: after the flow has been reversed, such particles need much more time to reach back the injection point than if they had stayed on the original flow line. The reverse effect is observed for particles located near the edges in the injection phase and diffusing towards a faster path in the pumping phase: there results an additional dispersion component which was not taken into account in the discussion leading to Eqs. 7 and 8.

A second possibility is due to transverse velocity gradients in the parallel part of the flow. Assume that the glass plates are not exactly parallel: since local velocity varies as the square of the local gap thickness, transverse velocity variations occur. Diffusion across these gradients induces additional dispersion which does not reverse when the flow direction is changed.

We shall now investigate both effects through Monte Carlo simulations. These simulations take into account both the Poiseuille velocity profile between the parallel smooth plates and molecular diffusion parallel and perpendicular to the flat plates. The effect of the transverse velocity gradient in a parallel flow will also be computed analytically in the Appendix.

4.1. Monte Carlo numerical simulation of echo dispersion

In these simulations (Bugliarello and Jackson, 1964), the tracer is assumed to be sufficiently diluted that tracer particles move independently of each other. One follows the 2-D displacement of a large number of particles moving in the Hele–Shaw cell. Initially ($t = 0$), all particles are released at a distance r_0 taken equal to 1 mm from the source at a height y_0. The starting positions on this circle are uniformly distributed according to the radial nature of the flow field close to the source. In order to reproduce the experimental conditions, the probability for a particle to start at a

given value of y_0 is modulated to follow the variations of the local flux of fluid with the Poiseuille profile. The motion of each particle is the combination of Brownian motion and convection.

We use the Hele–Shaw approximation: the local velocity is taken to be the product of a 2-D potential velocity field in the x–z-plane (Fig. 7) and the parabolic Poiseuille velocity profile between the plates. The 2-D potential field is given by (Milne-Thompson, 1968):

$$v_x(x,z) = \frac{U}{4}\left[\frac{\sinh(\pi x/b)}{\sinh^2(\pi x/2b) + \sin^2(\pi z/2b)}\right.$$

$$\left. + \frac{\sinh[\pi(x+2c)/b]}{\sinh^2[\pi(x+2c)/2b] + \sin^2(\pi z/2b)}\right] \tag{13a}$$

$$v_z(x,z) = \frac{U}{4}\sin(\pi z/b)\left[\frac{1}{\sinh^2(\pi x/2b) + \sin^2(\pi z/2b)}\right.$$

$$\left. + \frac{1}{\sinh^2[\pi(x+2c)/2b] + \sin^2(\pi z/2b)}\right] \tag{13b}$$

where $b = 50$ mm is the half width of the rectangular model and $c = 10$ mm the distance of the injection hole from the cell edge ($x = -c$). The flow lines shown in Fig. 7 have been computed from these formulas. The Hele–Shaw approximation is valid except very near the injection point and the rim of the model, because of the large ratio between the fracture aperture and its width. Note that this type of simulation can only be used in the case of smooth plates, since, for the rough model, the flow field is more complex and cannot be expressed analytically.

The positions of all particles are periodically updated with a time step Δt; Δt is chosen such that it is small when the particle velocities are high in order to keep the length of the convective displacements below a limiting value. The random Brownian motion is simulated by performing at each time-step a random jump of length $\sqrt{6D_m\Delta t}$ (Bugliarello and Jackson, 1964) where D_m is the molecular diffusion coefficient. The direction of the steps is random and distributed uniformly in all directions. The amplitude $\sqrt{6D_m\Delta t}$ of a random step has been chosen so that the variance of any coordinate after n independent steps of equal duration Δt would be:

$$\overline{[x(t) - x(0)]^2} = n \cdot 6D_m\Delta t \cdot \frac{1}{3} = 2D_m t \tag{14}$$

where the factor $\frac{1}{3}$ represents the variance of a random coordinate chosen uniformly on a unit sphere. Zero flux boundary conditions on the edges of the rectangular cell are implemented by reflecting the particles if they move outside the fluid volume. On the upper and lower surface of the cell, one uses a periodic boundary condition in which particles leaving at the top are reintroduced at the bottom: this does not introduce any bias because of the symmetry of the geometry and of the parabolic profile. The sequence of convective and diffusive displacements is pursued up to the inversion time T_{inv} after which the velocity U is replaced by $-U$ in Eqs. 13a and 13b. Then the process is repeated until the particles arrive within a distance r_0 from the

injection circle. The corresponding time represents the transit time of the particle. The process is repeated for a very large number of particles (up to 30,000). After all individual transit times have been recorded, one computes a "numerical" concentration variation curve $C(t)$ which is the fraction of particles with a transit time lower than t. This curve is analyzed with the same approach as that discussed above for the experimental results and fitted with solutions of the advection–diffusion equation. We have also computed directly the first and the centered second moments of the transit time distribution (for numerical simulations, the second moment can be computed directly since there is no signal drift and the initial and eventual values of the concentration are known exactly).

4.2. Numerical simulation results in the rectangular geometry

A first interesting feature is the fact that small deviations of the experimental curves from the Gaussian behaviour (Fig. 3a) are well reproduced in the simulations (Fig. 3b): these deviations appear as small leading and tailing trails. This is confirmed by the experimental and theoretical variations of the second moment σ_t^2 with T_{inv} which overlay perfectly (Fig. 8). In order to compare the values of σ_t^2 with the predictions of the Taylor model, we have plotted in Fig. 9a and b the variations of the ratio $\sigma_t^2/4T_{inv}\tau_m$ with T_{inv} (both for the Gaussian fit and the actual second moment of the numerical simulation curves). In a parallel flow with no longitudinal molecular diffusion, $\sigma_t^2/4T_{inv}\tau_m$ should reach a limiting value of $2/105$ at long times. At the highest flow rate $Pe = 356$ (Fig. 9a) the curves are nearly Gaussian and the ratio $\sigma_t^2/4T_{inv}\tau_m$ has the same value for the two types of fits: the limit at long times is slightly larger than the theoretical value from Eqs. 8 and 9 (0.022 against 0.019). The low values of $\sigma_t^2/4T_{inv}\tau_m$ at small times, such that $T_{inv} < \tau_m$, are not related to the particular geometry of the flow and are observed even in parallel flow geometries: this is due to the fact that the Taylor dispersion regime is not yet established (Taylor, 1953;
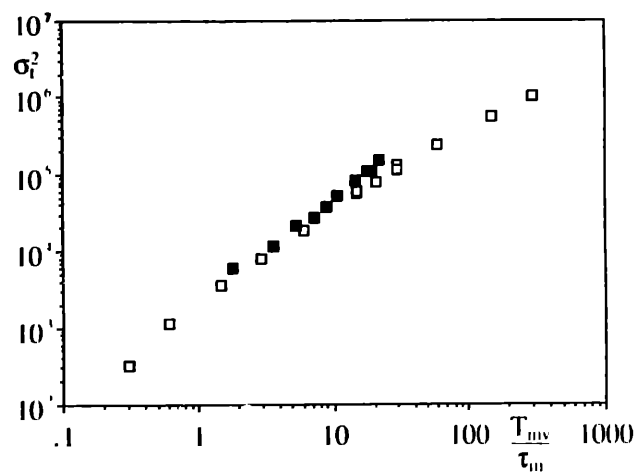

Fig. 8. Variation of the mean square transit time deviation σ_t^2 as a function of the ratio T_{inv}/τ_m for numerical simulations (□) and experiments (■) of echo dispersion in the same rectangular model fracture at the same Péclet number $Pe = 34$.
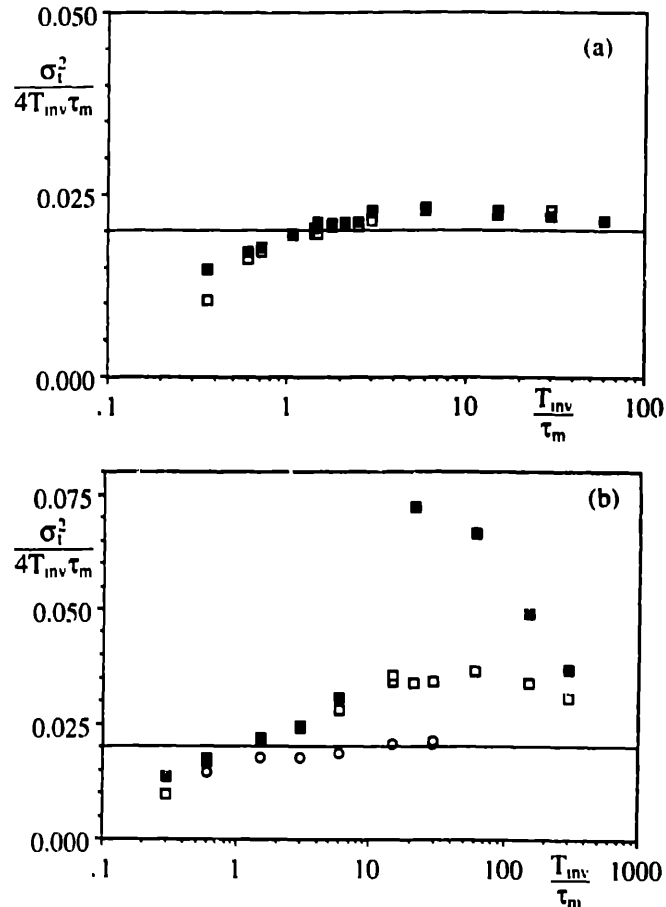
Fig. 9. Variation of the normalized transit time deviation $\sigma_t^2/4T_{inv}\tau_m$ as a function of the normalized injection time T_{inv}/τ_m for two Péclet number values:

a. Pe = 356 ($\square$ = values of $\sigma_t^2/4T_{inv}\tau_m$ for a fit of a solution of the advection-diffusion equation with the Gaussian part of the curve $C(t)$; $\blacksquare$ = direct computation of the $\sigma_t^2/4T_{inv}\tau_m$ from the numerical data).

b. Pe = 34 ($\square$ = values of $\sigma_t^2/4T_{inv}\tau_m$ for a fit of a solution of the advection-diffusion equation with the Gaussian part of the curve $C(t)$; $\blacksquare$ = direct computation of the $\sigma_t^2/4T_{inv}\tau_m$ from the numerical data; $\bigcirc$ = variation $\sigma_t^2/4T_{inv}\tau_m$ without molecular diffusion in the plane of the model).

Aris, 1956) so that the dispersion remains partly reversible. At the lower flow-rate Pe = 35.6 (square symbols in Fig. 9b), values of $\sigma_t^2/4T_{inv}\tau_m$ computed directly from the data points are markedly higher than those resulting from the "Gaussian" fit. This is due to the contribution of the front and rear "tail" parts. These values are 450% and 50% higher, respectively, than the theoretical ones.

In order to estimate the influence of diffusion across the flow lines we have performed numerical simulations in which molecular diffusion in the plane of the plates is suppressed (however, the flow field is kept identical, and molecular diffusion perpendicular to the plates, which is at the origin of Taylor dispersion, is retained). In this case (circles in Fig. 9b), the limiting value of $\sigma_t^2/4T_{inv}\tau_m$ is very close to the theoretical one corresponding to Taylor dispersion. This confirms the effect of molecular diffusion in the regions of high velocity gradients and near the edges of the model. We observe in Fig. 9b that $\sigma_t^2/4T_{inv}\tau_m$ does not return to the theoretical
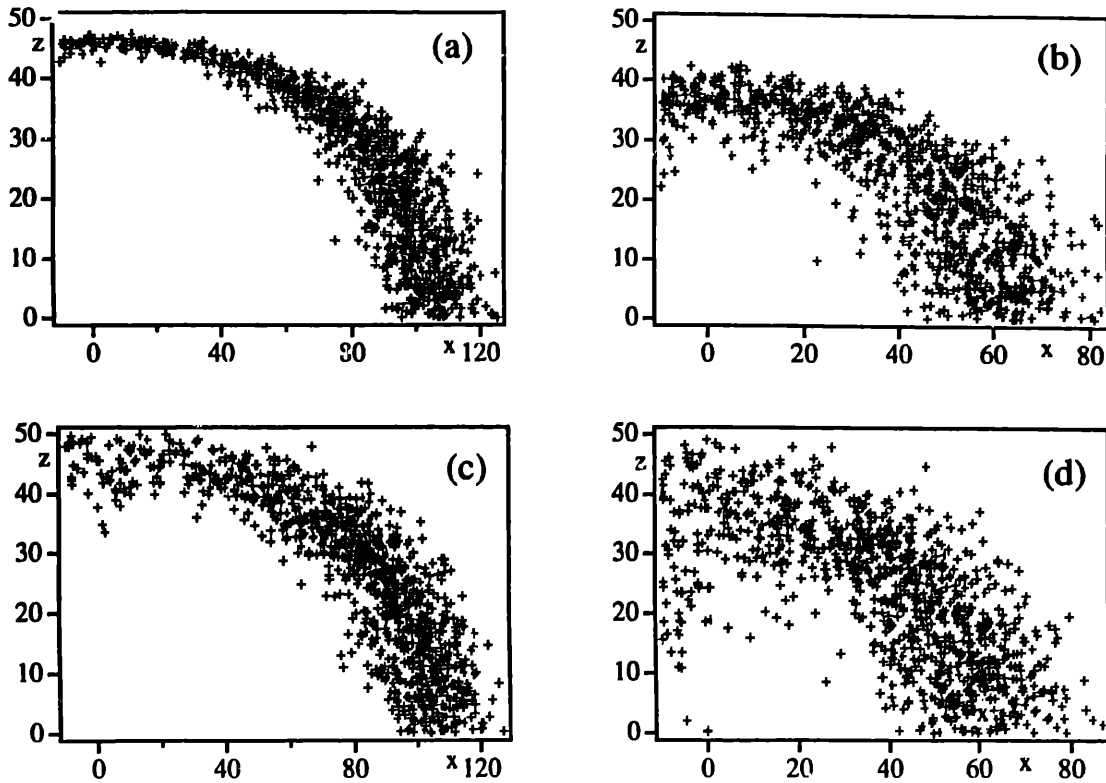
Fig. 10. Distribution of the location of 1000 tracer particles emitted during an echo experiment with $T_{inv} = 15\tau_m$ (= 2500 s) for a Péclet number Pe = 34.

a and b. Particle distributions without molecular diffusion in the plane of the model (molecular diffusion in the thickness is retained).

c and d. Particle distributions with molecular diffusion in the plane of the model.

The time lapse after particles emission is $t = 20\tau_m$ and $t = 25\tau_m$ for (a-c) and (b-d), respectively.

value even in the parallel part of the flow. To help understand this result, we have plotted the locations of the particles in the simulations without and with transverse diffusion. At the end of the injection phase, the particles are distributed over a very curved front (Fig. 10a and c): molecular diffusion transverse to the flow takes the particles ahead of the front and induces additional dispersion. At later times in the backflow phase, we observe more particles close to the injection point ahead of the main front when transverse molecular diffusion is included (Fig. 10d) than without including it (Fig. 10b).

4.3. Influence of transverse velocity gradients in the parallel flow

In this part, we concentrate on the influence of a transverse velocity gradient in the parallel velocity region of the Hele–Shaw cell. We assume that the plates are no longer parallel but make a small angle α with the apex of the wedge parallel to the flow [the local gap thickness is $a(z) = a_0 + z \, \mathrm{tg}\, \alpha$]. The velocity and constant-pressure lines remain parallel to Ox and Oz, respectively; if $v_x(0) = U$, the velocity deviation $\delta v_x(z) = v_x(z) - U$ satisfies $\delta v_x(z)/U = (z\,\mathrm{tg}\,\alpha)/a_0$. Since a tracer particle diffuses laterally by an amount $\delta z \approx \sqrt{D_m T_{inv}}$ during an experiment, the relative variations
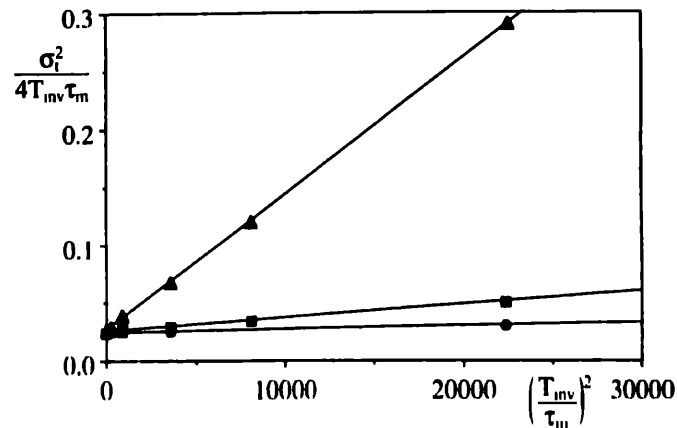
Fig. 11. Variation of $\sigma_t^2/4T_{inv}\tau_m$ with $(T_{inv}/\tau_m)^2$ for an echo dispersion in a parallel flow with a constant gradient of the cell thickness normal to the flow velocity [$\blacktriangle$: tg $\alpha = 6\cdot10^{-3}$; $\blacksquare$: tg $\alpha = 2\cdot10^{-3}$; : tg $\alpha = 1\cdot10^{-3}$ (α = angle between upper and the lower plane)].

δt of the transit time are given by: $\delta t/T_{inv} \approx \delta v_x(\delta z)/U$ so that the term $\sigma_t^2/4T_{inv}\tau_m$ should vary as:

$$\Delta(\sigma_t^2/4T_{inv}\tau_m) \propto \text{tg}^2\alpha(T_{inv}/\tau_m)^2 \tag{15}$$

We have verified this formula numericaliy with the Monte Carlo simulation technique reported above with a model width 50 mm and a mean thickness $a_0 = 1$ mm. The tracer particles were injected at $x = 0$ over the whole width of the model but with a probability proportional to the local flow-rate.

Fig. 11 displays the variation of the ratio $\sigma_t^2/4T_{inv}\tau_m$ with $(T_{inv}/\tau_m)^2$ for three angle values with tg $\alpha = 6\cdot10^{-3}$, $2\cdot10^{-3}$ and $1\cdot10^{-3}$. One indeed observes, particularly for the two largest gradients, a linear variation which extrapolates to a value 0.024, close to the value 0.022 for the combination of Taylor dispersion and molecular diffusion. The slopes are in the ratios 1, 0.096 and 0.023 which correspond well to the theoretical corresponding ratios 1, 0.111, 0.027 between the values of tg^2 α. We obtain:

$$\Delta(\sigma_t^2/4T_{inv}\tau_m) = (0.3 \pm 0.03)\text{tg}^2\alpha(T_{inv}/\tau_m)^2 \tag{16}$$

The value of the prefactor (0.3 ± 0.03) is in reasonable agreement with the analytical prediction obtained in the Appendix. In particular, for tg $\alpha = 6\cdot10^{-3}$, the numerical simulation yields a value of 0.325. Note that tg $\alpha = 6\cdot10^{-3}$ would correspond to an exceedingly large variation of 0.6 mm in the thickness of our spacers. A more realistic variation of 0.1 mm for our experiments (tg $\alpha = 10^{-3}$) would not give any measurable influence as shown in Fig. 11, even for very long transit times (10 h). However, the effect of variations in gap thickness may be important in practical applications.

We conclude from the numerical simulations that deviations from the Taylor predictions observed at low velocities can be accounted for by the complex shape of the flow field near the injection point. In addition, these velocity gradients induce a curvature of the front which results in some additional dispersion even when the parallel part of the flow has been reached. Velocity gradients transverse to the mean flow field have an effect increasing as the square of injection time but which

should be negligible in the range of thicknesses and transit time values which we have used.

5. Conclusions

We conclude from our results that echo tracer dispersion can be used to characterize the transport properties of 2-D structures in which fluid flows between parallel solid plates. Echo dispersion allows one to analyse local parameters such as the effective spacing between the walls or their roughness: in contrast, transmission dispersion in such geometries is generally controlled by macroscopic differences between the flow path lengths.

In parallel flows, the echo dispersivity is the sum of a geometrical term independent of the velocity U and of a Taylor-like term proportional to U. The former depends on the length scale of the asperities and dominates at low flow velocities; the latter becomes significant at high flow-rates and is controlled by the fracture aperture. Experiments performed on fractures with smooth parallel walls give markedly smaller low-velocity dispersivities than those measured with rough walls.

Using the echo dispersion technique allows one to eliminate much of the dispersion associated with macroscopic variations of the velocity. However, we have found experimentally and numerically that, at low velocities, molecular diffusion across the flow lines may induce additional dispersion when velocity gradients in the direction normal to the flow are present. In the geometry we have used, such gradients are present near the injection point and account well for the increase of the apparent dispersivity which we observed at low velocity. Variations in the gap thickness might also induce an increase of the apparent dispersivity as the square of the transit time: but this would however only occur at very long times in our experiments.

While the present work demonstrates that asperities of relatively uniform size give a dispersion component analogous to geometrical dispersion at low velocities, it will be important in the future to analyse the quantitative relation between the echo dispersion behaviour and geometrical parameters such as the aspect ratio of the asperities, their individual size and their spatial distribution. Another important point is the fact that recent experiments on both natural (Brown and Scholz, 1985; Schmittbuhl et al., 1993) and artificial (Bouchaud et al., 1990) materials have demonstrated that fracture surfaces have very often self-affine geometries with a very broad range of characteristic length scales. Self-affinity generalizes to anisotropic systems the statistical invariance of fractal structures with respect to changes of length scales and is therefore well adapted to the case of fractures: in these, displacements parallel and perpendicular to the mean fracture plane have different roles. This may have important implications on the transport properties of fractures such as their electrical conductivity or their permeability (Brown, 1987; Roux et al., 1993). It will be necessary to compare the dispersion characteristics of such multiscale systems with those of the structures which we studied above. Finally, some of the results which we have obtained may be generalized to dispersion for flow parallel to strata of porous

materials: in this case transverse hydrodynamic dispersion replaces molecular diffusion while the velocity variations across strata replace the parabolic velocity profile between the plates (Ackerer, 1987; Leroy et al., 1992).

Acknowledgements

Appendix — Taylor dispersion in a Hele–Shaw cell with a varying gap

Consider a flow in the x-y-plane in a Hele–Shaw cell with a slowly varying gap $h(x,y)$. The depth averaged velocity $u(u_x, u_y)$can be related to the local pressure gradient using the momentum equation for the viscous flow, and can also be expressed in terms of a stream function for the volume flux, i.e.:

$$u_x = -\frac{1}{h}\frac{\partial\psi}{\partial y} = -\frac{h^2}{12\mu}\frac{\partial p}{\partial x} \tag{A-1a}$$

$$u_v = -\frac{1}{h}\frac{\partial\psi}{\partial x} = -\frac{h^2}{12\mu}\frac{\partial p}{\partial y} \tag{A-1b}$$

The stream function and pressure therefore form an orthogonal coordinate system. In terms of this coordinate system, the advection–diffusion equation for a concentration C with different diffusivities parallel and perpendicular to the flow takes the form:

$$\frac{\partial C}{\partial t} - \frac{12\mu u^2}{h^2}\frac{\partial C}{\partial p} = \frac{u^2}{h}\left[\frac{\partial}{\partial p}\left(D_\parallel \frac{144\mu^2}{h^3}\frac{\partial}{C\partial p}\right) + \frac{\partial}{\partial\psi}\left(D_\perp h^3 \frac{\partial C}{\partial\psi}\right)\right] \tag{A-2}$$

It is now convenient to make a further coordinate transformation in the streamline direction to a Lagrangian variable moving with the flow. Along the streamline $y = $ const., the pressure changes according to:

$$\dot{p} = \dot{x}.\nabla p = -12\mu u^2/h^2 \tag{A-3}$$

Let $p = P(t,)$ be the solution of this equation with the initial condition $p = 0$ at $t = 0$.

Now transform from the variables t, p and ψ to the variables t, s and ψ, respectively, with s defined by $p = P(t - s, \psi)$, i.e. the time the fluid element passed through $p = 0$. In the echo experiment, this new variable s is equal to the return time for a fluid element relative to the mean return time.

In terms of the new variables the advection–diffusion equation becomes:

$$\frac{\partial C}{\partial t} = \frac{u^2}{h}\left[\frac{h^2}{u^2}\frac{\partial}{\partial s}\left(D_\parallel \frac{1}{hu^2}\frac{\partial C}{\partial s}\right) + \left(\frac{\partial}{\partial\psi} - \Theta\frac{\partial}{\partial s}\right)\left\{D_\perp h^3\left(\frac{\partial C}{\partial\psi} - \Theta\frac{\partial C}{\partial s}\right)\right\}\right] \tag{A-4}$$

where $\Theta = P_\psi h^2/12\mu u^2$.

We now make the thin pulse approximation. At high Péclet numbers an initial release of a delta function of concentration simultaneously on all of the streamlines $C(x,y,t) = \delta(s)$ at $t = 0$ for all ψ will spread little as it is advected rapidly.

There will thus be high gradients of C for changes in s, but slow changes in C with respect to ψ. Also D, u, h and P_ψ will vary slowly in t, s and ψ. The spreading of the thin pulse is therefore governed by:

$$\partial C\partial t = \left(\frac{D_\parallel}{u^2} + \frac{D_\perp h^6 P_\psi^2}{144\mu^2 u^2}\right)\frac{\partial^2 C}{\partial s^2} \tag{A-5}$$

where the bracket is to be evaluated at $s = 0$ and will be a function of t and ψ. The factor u^2 dividing $D_\parallel$

represents a spatial "piling up" of the advected information as the velocity reduces. The $h^3 P_\psi / 12\mu$ term represents the shear between adjacent streamlines, producing gradients across streamlines and hence a diffusion to different s on those streamlines. Note that this effect is small at very high Péclet numbers with smooth walls because Taylor dispersion makes $D_\perp \ll D_\parallel$.

We now apply this general theory to the simple case of flow in the x-direction with the gap $h(y)$ between the plates varying across the flow. Writing $G = (\mathrm{d}p/\mathrm{d}x)/12\mu$, we have $u = h^2 G = h^{-1}\psi_y$ so:

$$\psi(y) = \int_0^y h^3(y')G\mathrm{d}y' \quad \text{and} \quad P(t,\psi) = -12\mu h^2(y)G^2 t$$

which gives

$$P_\psi = P_y/\psi_y = -24\mu h' G t/h^2$$

Thus:

$$D_\parallel + D_\perp h^6 P_\psi^2/144\mu^2 = D_\parallel + D_\perp 4h'^2 u^2 t^2/h^2 \tag{A-6}$$

Hence for a significant effect one needs the parallel and perpendicular diffusivities to be comparable, as for instance with rough plates or smooth plates at moderately high Péclet numbers $O(10)$. Also, the displacement ut must be comparable with the distance h/h' over which the gap varies significantly.

For an echo experiment of injecting for time T_{inv} and then withdrawing at the same constant rate, the spread of the return times is predicted by the thin pulse approximation to be:

$$\frac{\Delta t_r^2}{2T_{inv}} = \frac{D_\parallel(u) + D_\perp 16h'^2 u^2 T_{inv}^2/3h^2}{u^2} \tag{A-7}$$

which is in agreement with the numerical simulations in Section 4 (Eq. 16).

References

Ackerer, P., 1987. Random-walk model to simulate pollutant transport in alluvial aquifers or fractured rocks. In: E. Custodio, A. Gurgi and J.P. Lobo Ferreira (Editors), Advances in Analytical and Numerical Ground Water Flow and Quality Modeling. NATO (N. Atlantic Treaty Org.) ASI (Adv. Stud. Inst.). Ser. 224, Ser. C, Reidel, Dordrecht.

Aris, R., 1956. On the dispersion of a solute in a fluid flowing through a tube. Proc. R. Soc. London, Ser. A, 235: 67–77.

Bear, J., 1972. Dynamics of Fluids in Porous Media. American Elsevier, New York, NY, 764 pp.

Bouchaud, E., Lapasset, G. and Planès, J., 1990. Fractal dimension of fractured surfaces: a universal value? Europhys. Lett., 13: 73–79.

Brown, S.R., 1987. Fluid flow through rock joints, the effect of surface roughness. J. Geophys. Res., 92: 1337–1347.

Brown, S.R. and Scholz, C.H., 1985. Broad bandwidth study of the topography of natural rock surfaces. J. Geophys. Res., 90: 12575–12582.

Bugliarello, G. and Jackson, E.D., 1964. Random walk study of convective diffusion. Proc. Am. Soc. Civ. Eng., J. Eng. Mech. Div., EM 4, pp 49–77.

Charlaix, E., Guyon, E. and Rivier, N., 1984. A criterion for the percolation threshold in a random array of disks. Solid State Commun., 50: 999–1002.

Charlaix, E., Guyon, E. and Roux, S., 1987. Permeability of an array of fractures with randomly varying apertures. Transport Porous Media, 2: 31–43.

Charlaix, E., Hulin, J.P., Zarcone, C. and Leroy, C., 1988. Experimental study of tracer dispersion in flow through two-dimensional networks of etched capillaries. J. Phys. D, Appl. Phys., 21: 1727–1732.

Dullien, F.A.L., 1979. Porous Media, Fluid Transport and Pore Structure. Academic Press, New York, NY, 396 pp.

Evans, K.F., Kohl, T., Hopkirk, R.J. and Rybach, L., 1992. Modelling of energy production from hot dry rock systems. Natl. Energie Forsch. Fonds Proj. 359. Polytech. School Zürich, Zürich, Fin. Rep., 316 pp.

Fried, J.J. and Combarnous, M.A., 1971. Dispersion in porous media. Adv. Hydrosci., 7: 169–282.

Hulin, J.P. and Plona, T.J., 1989. "Echo" tracer dispersion in porous media. Phys. Fluids, A1: 1341–1347.

Koplik, J., 1988. Hydrodynamic dispersion in random networks. In: E. Guyon, J.P. Nadal and Y. Pomeau (Editors), Disorder and Mixing, Ch. 7. Kluwer, Dordrecht, pp. 123–137.

Kurowski, P., Ippolito, I., Koplik, J., Hinch, E.J. and Hulin, J.P., 1994. Anomalous tracer dispersion in a dipole flow geometry. Phys. Fluids A, 6: 108–117.

Leroy, C., Hulin, J.P. and Lenormand, R., 1992. Tracer dispersion in stratified porous media: influence of transverse dispersion and gravity. J. Contam. Hydrol., 11: 51–68.

Levenspiel, O., 1972. Chemical Reaction Engineering. Wiley, New York, NY, Ch. 9.

Milne-Thompson, L.M., 1968. Theoretical Hydrodynamics. Macmillan, New York, NY, 660 pp.

Moreno, L., Tsang, Y.W., Tsang, C.F., Hale, F.V. and Neretnieks, I., 1988. Flow and tracer transport in a single fracture: a stochastic model and its relation to some field observations. Water Resour. Res., 24: 2033–2048.

Pfannkuch, H.O., 1963. Contribution à l'étude des déplacements de fluides miscibles dans un milieu poreux. Rev. Inst. Fr. Pét., 18: 215–270.

Roux, S., Schmittbuhl, J., Vilotte, J.P. and Hansen, A., 1993. Some physical properties of self-affine rough surfaces. Europhys. Lett., 23: 277–282.

Saffman, P.G., 1959. A theory of dispersion in porous media. J. Fluid Mech, Part III, 6: 321–349.

Schmittbuhl, J., Gentier, S. and Roux, S., 1993. Field measurements of the roughness of fault surfaces. Geophys. Res. Lett., 20: 639–641.

Silliman, S.E., 1989. An interpretation of the difference between aperture estimates derived from hydraulic and tracer tests in a single fractures. Water Resour. Res., 25: 2275–2283.

Taylor, G.I., 1953. Dispersion of soluble matter in solvent flowing slowly through a tube. Proc. R. Soc. London, Ser. A, 219: 186–203.